METRICA
METRology Institutional CAtalog

ISTITUTO NAZIONALE DI RICERCA METROLOGICA
Repository Istituzionale

Liquid Crystalline Network Microstructures for Stimuli Responsive Labels with Multi-Level Encryption

(Article begins on next page)

09 May 2024

Liquid Crystalline Network Microstructures for Stimuli Responsive Labels with Multi-Level Encryption

Simone Donato, Sara Nocentini, Daniele Martella,* Srikanth Kolagatla,
Diederik S. Wiersma, Camilla Parmeggiani, Colm Delaney,* and Larisa Florea*

Two-photon direct laser writing enables the fabrication of shape-changing microstructures that can be exploited in stimuli responsive micro-robotics and photonics. The use of Liquid Crystalline Networks (LCN) allows to realize 3D micrometric objects that can contract along a specific direction in response to stimuli, such as temperature or light. In this paper, the fabrication of free-standing LCN microstructures is demonstrated as graphical units of a smart tag for simple physical and optical encryption. Using an array of identical pixels, information can be hidden to the observer and revealed only upon application of a specific stimulus. The reading mechanism is based on the shape-change of each pixel under stimuli and their color that combine together in a two-level encryption label. Once the stimulus is removed, the pixels recover their original shape and the message remains completely hidden. Therefore, an opto-mechanical equivalent of an "invisible ink" is realized. This new concept paves the way for introducing enhanced functionalities in smart micro-systems within a single lithography step, spanning from storage devices with physical encryption to complex motion actuators.

S. Donato, S. Nocentini, D. Martella, D. S. Wiersma, C. Parmeggiani
European Laboratory for Non Linear Spectroscopy (LENS)
via N. Carrara 1, Sesto Fiorentino 50019, Italy
E-mail: d.martella@inrim.it

S. Donato, D. S. Wiersma
Department of Physics and Astronomy
University of Florence
via G. Sansone 1, Sesto Fiorentino 50019, Italy

S. Nocentini, D. Martella, D. S. Wiersma
Istituto Nazionale di Ricerca Metrologica (INRiM)
Strada delle Cacce 91, Torino 10135, Italy

D. Martella, C. Parmeggiani
Department of Chemistry "Ugo Schiff"
University of Florence
via della Lastruccia 3–13, Sesto Fiorentino 50019, Italy

S. Kolagatla, C. Delaney, L. Florea
School of Chemistry & AMBER
The SFI Research Centre for Advanced Materials and BioEngineering Research
Trinity College Dublin
Dublin 2, Ireland
E-mail: cdelane5@tcd.ie; floreal@tcd.ie

1. Introduction

Miniaturization of responsive polymers is currently gaining attention due to its potential application in a variety of fields. Smart materials, which respond to external stimuli with a reversible shape-change, are essential elements of new actuators to be employed in microfluidics,[1–3] photonics,[4] and micro-robotics.[5–8]

These functional devices exploit the so-called 4D printing in which 3D architectures are able to change their properties under a proper stimulus.[9] In this context, Direct Laser Writing (DLW) by two-photon polymerization represents a versatile solution for 4D additive manufacturing at length scales ranging from nano to micrometers.[10–12] Recently, this technology has been adapted for the fabrication of stimuli-responsive materials, such as hydrogels, on the microscale.[13,14] These systems can generate actuation by reversible swelling and deswelling in aqueous media in response to a physical stimulus[15,16] (e.g., above or below a low critical solution temperature) or chemical ones (e.g., in response to solvent polarity or sugar concentration).[17,18] However, for a wider range of applications, materials that can actuate themselves in a programmable way, both in air or in different liquids, would be of much benefit. Additionally, achieving anisotropic deformation is higly demanded for application design. Both these aspects find a solution in the use of Liquid Crystalline Networks (LCNs) that represent one of the most suitable candidates for smart artificial devices,[19] owing to their ability to deform in response to temperature variations,[20] light,[21,22] magnetic[23] or electric fields.[24] LCNs combine the anisotropic features of Liquid Crystals (LCs) with the mechanical behavior of polymeric networks.[25,26] The first LCNs 3D patterned with DLW were based on nematic monomers,[27] where the molecules possess only one degree of orientational order. Upon transition from the liquid crystal to the isotropic phase, a (partial) disordering of the mesogenic units triggers the polymer deformation with a contraction along the director (and an expansion in the perpendicular plane). Reversible actuation is achieved upon removal of the stimulus[26] and different deformations (such as bending or twisting) can be engineered by programming the LC alignment.[28]

The use of DLW with acrylate-based reactive mesogens has been already demonstrated to generate simple robotic operations

**ADVANCED
SCIENCE NEWS**

www.advancedsciencenews.com

NANO · MICRO

small

www.small-journal.com

(such as for micro-hands[29] or micro-walkers[30]), to realize photonic devices (such as diffraction gratings[31] or elastic woodpiles[32]) and opto-mechanical metamaterials.[33] Fabrication of free standing structures with maximum resolution of 160 nm has been demonstrated.[34] In all the examples, light actuation has been controlled thanks to an azobenzene dye inserted in the polymeric chains before the polymerization [27] or after it by post functionalization method.[35] Also LC microstructures with structural color have been obtained by the use of cholesteric photoresists.[36,37]

To design the properties of LCN microstructures, DLW requires a careful evaluation of two fundamental aspects related to the monomer formulation and printing parameters. Regarding the former, the use of cross-linkers having different steric hindered substituents allows to modulate the weak interaction among LC cores, therefore affecting the actuation and mechanical performances of the polymeric systems.[38] At present, this aspect is barely analyzed for 3D printed microstructures, whereas a more common way to control the deformation (extent of contraction and speed of the response) is to change the cross-linker percentage.[39]

On the other hand, a general and more convenient route to modify the microstructures properties is the use of a gray-scale lithographic approach that consist in a careful spatial modulation of the light dose during printing.[40] Lower laser powers lead to a decrease of the cross-linking degree and consequently enable larger deformations during the actuation.[41] This method has been successfully demonstrated also for hydrogels where, combining regions with different cross-linking density in a single fabrication step, led to complex motions during deswelling.[42,43]

In this work, we describe both a chemical approach (changing the cross-linker substituent) and a lithographic one to modulate the shape-changing properties of LCN microstructures. In this way, we found a simple method to combine active deformable elements with different responses (under a constant stimulus) using only one optimized monomer formulation. This combination represents an efficient way to realize reconfigurable pixelated arrays based on a single photoresist. We believe that this advancement will be fundamental in broadening the application of active microstructures, to encode information using physical and miniaturized labels.[44]

As a first simple prototype, we demonstrated a micrometric tag with a code that is invisible except under certain environmental conditions.[45,46] During DLW, hidden information (in this case a letter) has been encoded in elementary units assembled in a 2D array. The elements are indistinguishable from the outside and only using an appropriate reading mechanism, e.g. applying a certain temperature or light dose, they respond differently to show the physical (hidden) data. A second decoding mechanism is possible by observation with polarized light exploiting the birefringence of LCN pixels, allowing to create a multi-level reading of the encryption array.

2. Result and Discussion

Different LCN microstructures were prepared by DLW with a two-photon polymerization. In this technique, a near-infrared laser (780 nm) is directly focused into a photoresist inserted in an LC cell, as illustrated in **Figure 1**A. When the laser intensity exceeds a certain threshold, the photo-polymerization begins, leading to the formation of a solid nano-volume with an ellipsoidal shape (voxel with minor axis dimension ≈150 nm and major axis of 400 nm).

The structure of the mesogenic monomers is reported in Figure 1B. A mono-acrylate mesogen (C6BP), a diacrylate cross-linker, a photo-initiator (PBPO), and an azobenzene dye have been included in each formulation. All the mixtures contained 20% mol/mol of a cross-linker, 1% mol/mol of photo-initiator, and 1% mol/mol of dye.
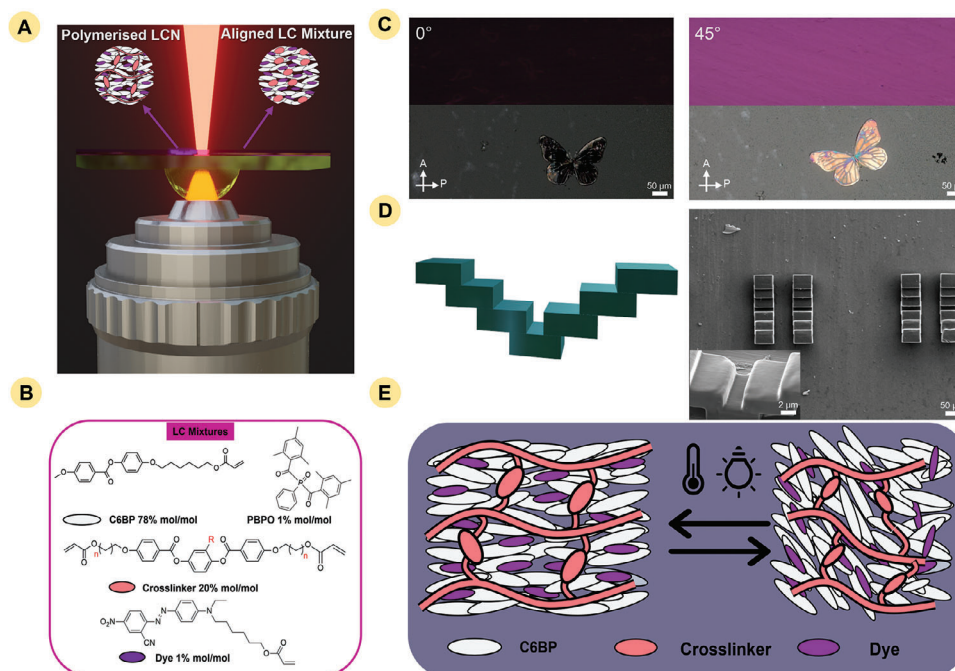
The structure of the reactive cross-linker has been changed in order to optimize the polymer mechanical properties, while the other components remained unchanged. In this study, the cross-linkers are named as CLX-Y, where X is the number of carbon atoms in the alkyl spacer and Y is the substituent on the central aromatic ring. For example, CL3-Me indicates the cross-linker with a propyl spacer between the core and the acrylate group and a methyl (Me) substituent in the aromatic ring. Accordingly, the monomer mixture and the final materials are referred to as LCNX-Y. CL3-Me and CL6-Me differ only in the length of the spacer (three or six carbon atoms in the flexible chain), whereas CL6-Ph presents a bulkier lateral group (the phenyl one) that increases the steric hindrance. Previous researches on macroscopic LCN films revealed that the presence of sterically hindered substituents weakened the energy between the LC cores, impacting the actuation performance of systems.[38,47,48]

The monomers were homogeneously mixed and infiltrated by capillary force inside a LC cell to obtain the desired alignment at room temperature. The cells were assembled using two glass coverslips coated with a polyimide sacrificial layer that is unidirectionally rubbed with a velvet cloth. In this way, we obtained a monodomain planar alignment of the mesogens along the rubbing direction.

The good quality of the alignment was confirmed by Polarized Optical Microscopy (POM) as shown in Figure 1C. During this measurement, extinction of transmitted light was observed when the cell director was placed parallel or orthogonal to the fast axis of the microscope polarizers, while the maximum transmission was observed at an angle of $\pi/4$ in between the director and the fast axis of the cross polarizers. This provided a clear indication of the alignment reached by the LC cells and also maintained in the printed structures (such as the butterfly in Figure 1C).

Using different mixtures, free-standing 3D objects were printed using DLW on one surface of the aligned cell and subsequently developed in isopropanol to remove the unpolymerized monomers. Scanning Electron Microscope (SEM) images in Figure 1D show different four-step stairs printed using LCN3-Me photoresist, demonstrating the possibility to obtain suspended features.

For the microstructures, a gradual disordering of the mesogenic units can be triggered under application of stimuli, generating a reversible shape-change and therefore 4D microstructures. The temperature sensitivity of the LC materials results in reversible contractions under heating (Figure 1E). Alternatively, deformation can be achieved by light irradiation when azobenzene dye are inserted in the polymer. In this case, the shape-change is driven by the *trans-cis* isomerization of the chromophore and/or light dissipation into heat.[49–52]

**ADVANCED
SCIENCE NEWS**

www.advancedsciencenews.com

NANO · MICRO

small

www.small-journal.com

Figure 1. DLW of LCN microstructures. A) Scheme of DLW two-photon polymerization in oil immersion configuration for a LC cell; B) Chemical structures of the acrylate monomers exploited; C) Observation of the homogeneous planar alignment in LC cells and polymeric structures analyzed by POM. Images are taken at 0° and 45° with respect to the main alignment director; D) Example of a four step-stair design and SEM images of printed microstructures; E) Schematic illustration of the resulting network and its reversible contraction under temperature or light irradiation.

Mesomorphic properties of the photoresists were investigated using Differential Scanning Calorimetry (DSC) and POM, as shown in **Figure 2**A,B for LCN6-Ph mixture. During the first heating cycle of the calorimetric investigation, the photoresist showed only one endothermic peak. This can be attributed to melting from the crystal to a (isotropic) liquid phase. During the cooling cycle, one exothermic peak was detected suggesting an isotropic (liquid) to LC phase transition. POM observation of the Schlieren texture (depicted in Figure 2B with typical 4- and 2-branches defects) were used to attribute this mesophase to a nematic phase.[53] Similar characterizations have been performed for the other photoresists and reported in Figures S1–S3 (Supporting Information). Transition temperatures were summarized schematically in Figure 2C.

All photoresists showed a monotropic behavior (with nematic phase observed only on cooling) and exhibited a LC phase at room temperature, with no crystallization recorded for several days after the first melting. This property enables easy processing of the material at room temperature and integration into 3D printing and lithographic techniques.[54] Upon increasing the aliphatic chain length in the cross-linker (from CL3-Me to CL6-Me) the nematic-to-isotropic transition temperature (T_{N-I}) increases (from 57 to 63 °C), whereas increasing steric hindrance in the core (from CL6-Me to CL6-Ph) reduces T_{N-I} to 39 °C. All the mixture showed similar enthalpies associated with the LC to isotropic phase transition (Table S1, Supporting Information).

According to previous studies on macroscopic LCN films,[38] we verified how the cross-linker structure affects the thermomechanical properties. Macroscopic LCN films have been characterized by DSC and representative traces are reported in Figure 2D.

As expected, it was not possible to define a clear nematic to isotropic phase transition and only a glass transition was observed. Increase of flexible spacer had a negligible effect on glass transition temperature (T_g), from 20 to 19 °C, while increasing the steric hindrance on the aromatic core (from methyl to phenyl group), lowered the T_g to 13 °C. To better highlight the effect of this central substituent, a Dynamic Mechanical Analysis on LCN6-Me and LCN6-Ph is reported in Figure S4 and Table S2 (Supporting Information) showing the storage modulus (E') and T_g during a heating cycle. For both samples, E' followed a typical downward passing from a glass state to a rubber one by increasing the temperature. At room temperature, E' decreased from ≈1900 to 400 MPa by increasing the steric hindrance.

The mixtures were then employed to realize microstructures with different 3D architectures presented in **Figure 3**A. The design included a bulk planar structure (directly linked to the surface), a suspended block on a cubic pedestal (called later table) and more complex elements (e.g., stairs with different number of suspended steps). For each photoresist, a careful evaluation of the optimized printing conditions was performed, with additional information discussed in the Experimental Section. All the designs shown in Figure 3A were printed in all the mixtures. The fidelity between the design and the resulting structure was evaluated by SEM and Atomic Force Microscopy (AFM). For the latter, the height profile measured for the case of a three-step stair design is contained in Figure S5 (Supporting Information), showing good reproducibility of the design during the printing.

In general, we observed that the change of slicing and hatching distances (that are respectively the separation between two

ADVANCED
SCIENCE NEWS
www.advancedsciencenews.com

NANO · MICRO
small
www.small-journal.com
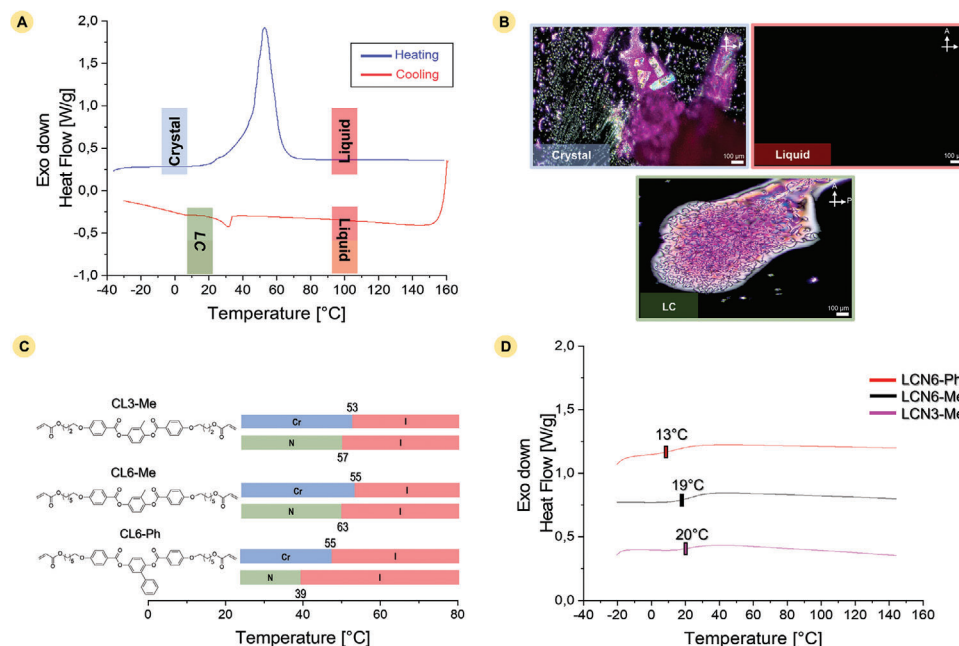
Figure 2. Characterization of the mesomorphic properties of LC mixtures and polymerized films. A) DSC trace of the first heating-cooling cycle of LCN6-Ph mixture (20 °C min^{-1}); B) Representative POM images of LCN6-Ph mixture in the crystal, nematic and isotropic liquid phases; C) Summary of the transition temperatures for the photoresists determined by the first DSC heating-cooling cycle (20 °C min^{-1}): Cr: crystal phase; N: Nematic phase; I: Isotropic phase. All temperatures are taken at the maximum of the transition peak. D) DSC traces of bulk LCN films during the first heating cycle (20 °C min^{-1}).

consecutive layers and two consecutive beam scans in the plane) have a smaller effect on the final structures than that of laser power, scan speed, and geometry design. The optimized parameters to obtain well defined microstructures were 40 mW as laser power (LP) and 10 mm s^{-1} as scan speed (SS), for LCN3-Me and LCN6-Me, and 50 mW and 10 mm s^{-1} for LCN6-Ph. For the latter, a slightly higher power was needed as suggested also by its softness with respect to the other mixture.

The shape-change owed to thermal-actuation was investigated across several heating-cooling cycles. An example of the thermo-actuation of a micro-stair prepared by LCN3-Me is reported in Figure 3B. The graph reports the contraction (C_T) at different temperatures, as defined by the following Equation (1):

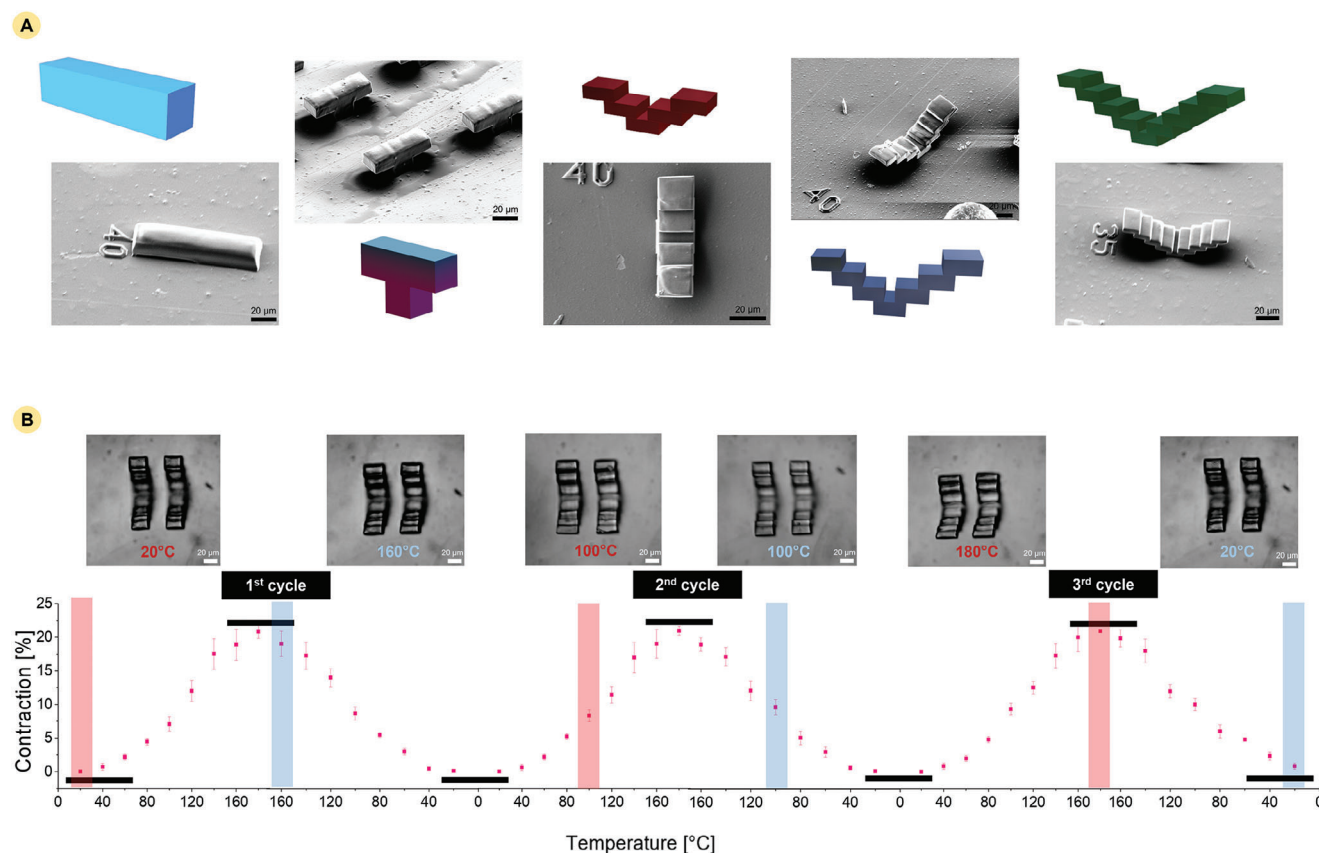$$C_T \; [\%] = \left(\frac{L_0 - L_f}{L_0} \right) \times 100 \tag{1}$$

where L_0 and L_f are the lengths measured respectively at room temperature and at a specific temperature (during heating or cooling) of the object considered. Each L_0 and L_f was measured for different structures in three different positions as shown in Figure S6 (Supporting Information). As expected, during heating, a gradual contraction was obtained along the nematic director. The contraction was obtained starting from 40 °C and, at 180 °C, a maximum shrinkage of 21% ± 1% was obtained. As it cooled, the structure followed the reverse evolution of shape, with the length of the scale gradually increasing until it recovered its original shape ≈40 °C. By repeating the heating and cooling cycles (3 cycles are shown in Figure 3B), the process was demonstrated to be totally reversible. To be noted that the actuation data

reported in this article (Figures 3 and 4) are given as a medium contraction measured on ten structures printed with the same parameters, demonstrating the high reliability of the fabrication process and material chosen.

Engineering the material deformation under stimuli is one of the most important parameters to develop application in soft robotics and photonics where a precise control on the (3D) shape under stimuli is needed. In general, improving the contraction, decreasing the temperature needed for the actuation, and combining parts that deform differently are the three main goals in developing new polymeric actuators.

Toward these objectives, an investigation of thermally-induced contraction has been reported in **Figure 4** trying to understand possible contributions due to the different mixtures and printing parameters. The study has been conducted on structures with less complexity than the stairs but still preserving suspended elements. In particular, we analyzed "tables" consisting of a simple block suspended on one cubic central pedestal. Figure 4A depicts optical microscope (bright field) images of a micro-table taken at specific temperatures during the heating cycle, while Figure 4B shows the graph comparing the thermal-actuation of structure written under the same conditions (40 mW as laser power and 10 mm s^{-1} as scan speed) but using the different mixtures. Also in this case, the contraction values were determined by optical images following the procedure illustrated in Figure S7 (Supporting Information).

This finding demonstrates that LCN6-Ph has considerably superior actuation qualities than the other materials with a maximum contraction at 180 °C of 27% ± 1% (with respect to 15% ± 1% for LCN3-Me and 14% ± 2% for LCN6-Me).

**ADVANCED
SCIENCE NEWS**

www.advancedsciencenews.com

**NANO · MICRO
small**

www.small-journal.com

Figure 3. Examples of LCN microstructures with different design and reversibility of thermal actuation. A) Design and SEM images for different geometries (blocks, tables and stairs); B) Optical microscope images and graphs of contraction during a thermal actuation test (from 20 to 180 °C) for four-step-stairs fabricated by LCN3-Me. Error bars indicate the standard deviation for each point.

Interestingly, the graph demonstrated that we are able to print the same micron-sized structure in all the photoresists but obtaining differences in shape under temperature actuation. This should allow the production of microstructures with different deformation under a constant stimulus by sequential fabrication steps of LC photoresists.[55]

However, this preparation method would employ multiple writing steps, multiple solvent developments and multiple alignment procedures. Achieving differential deformations in structures made by a unique writing step[43] will open to easier integration of devices.

Towards this objective, we studied the possibility of obtaining a gray-scale actuation (i.e., a different contraction under the same flat stimulus) for microstructures prepared by a single resist. Micro tables have been prepared within the photoresist that offers the greatest contraction (LCN6-Ph), employing different writing parameters (gray-scale lithography approach). Examples of the thermal contraction produced by this gray-scale approach have been reported in Figure 4C.
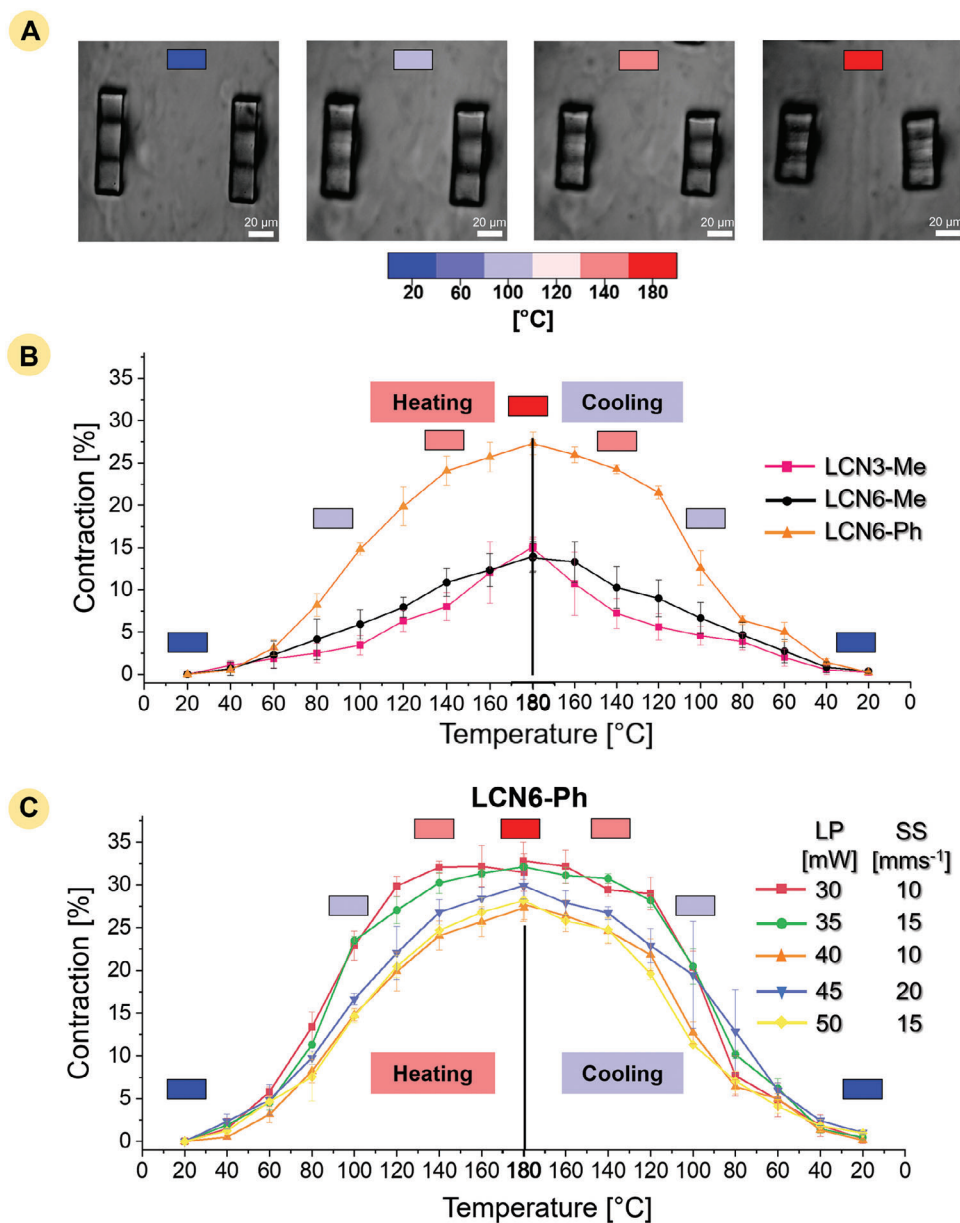
As can be observe, the curve trends are all comparable, but the extent of the contraction can be programmed using the printing parameters. In particular, the tables produced with 30 mW laser power and 10 mm s^{-1} scan speed exhibited a the maximum shrinkage of the series (32% at 180 °C) with the most notable difference being observed above 120 °C. This means that to obtain

an appreciable gray-scale actuation a certain temperature threshold has to be overcome.

Analysing only one writing parameter, we observed as the maximum contraction decreased by increasing the laser power (at the same scan speed) probably due to an increased cross-linking density.[41,56] Even if the contraction difference within this approach is smaller than the one obtained combining different photoresists, the easy integration of these structures should be applied in devices that need multiple shape-changing elements in an integrated systems. An example should be a physical encoding device where a digital information is hidden in the material pixel properties (e.g., shape, color).

For a clearer comparison of the actuating properties, other details related to the effect of the cross-linker percentage (Figure S8 and Table S3, Supporting Information) and microstructure shape (Table S4, Supporting Information) are reported in Supporting Information. In general, a higher cross-linker content leads to smaller deformation, while the substrate strain can influence the contraction of structures prepared by the same material and parameters. For this reason, all the comparisons already presented have been made using the same geometry and dimension of a suspended design (to reduce the strain and increase the possible deformation).

A proof-of-concept for encryption and physical decoding of basic information (in this case a letter) using LCN microstructures

2306802 (5 of 10)

ADVANCED
SCIENCE NEWS

www.advancedsciencenews.com

NANO · MICRO
small

www.small-journal.com

Figure 4. Comparison of thermal deformation for LCN microstructures prepared with different monomer mixtures and printing parameters. A) Bright field images of LCN6-Ph tables at different temperatures; B) Comparison of contraction reached by micro tables realized with different photoresists (and printed using 40 mW LP and 10 mm s^{-1} SS); C) Comparison of contraction reached by micro tables realized with LCN6-Ph mixture at various laser powers and scan speeds. Error bars shown in the graphs are referred to the standard deviation of the data represented for the same structure (same parameters) printed several times.

is reported in **Figure 5**. The letter was codified in a matrix of 20 pixels (five columns by four rows) that are initially indistinguishable (the letter was hidden) as depicted in Figure 5A. However, the binary elemental units can be differentiated by their response to thermal stimuli. For example, the array can be prepared with materials that have different contractions under temperature variation, thus the thermal stimulus can be used to obtain different shapes between the pixels to reveal the letter. The pixels in Figure 5 are called as "1" (with larger deformation) or "0" (with minor or no deformation).

In the first example (Figure 5B), a letter has been encrypted in the array of pixels prepared by a multi-material fabrication to combine LCN microstructures with a non-responsive commercial photoresist (IP-L 780) in a two-step protocol. The micro table design has been taken as basic elements and the two materials were printed under identical experimental conditions (50 mW LP and 10 mm s^{-1} SS). In the first step, the LC microstructures were printed and developed. Afterward, the other pixels were fabricated using IPL-780. As shown, the final array was composed of multi-material structures without any discernible difference

ADVANCED
SCIENCE NEWS

www.advancedsciencenews.com

NANO · MICRO

small

www.small-journal.com
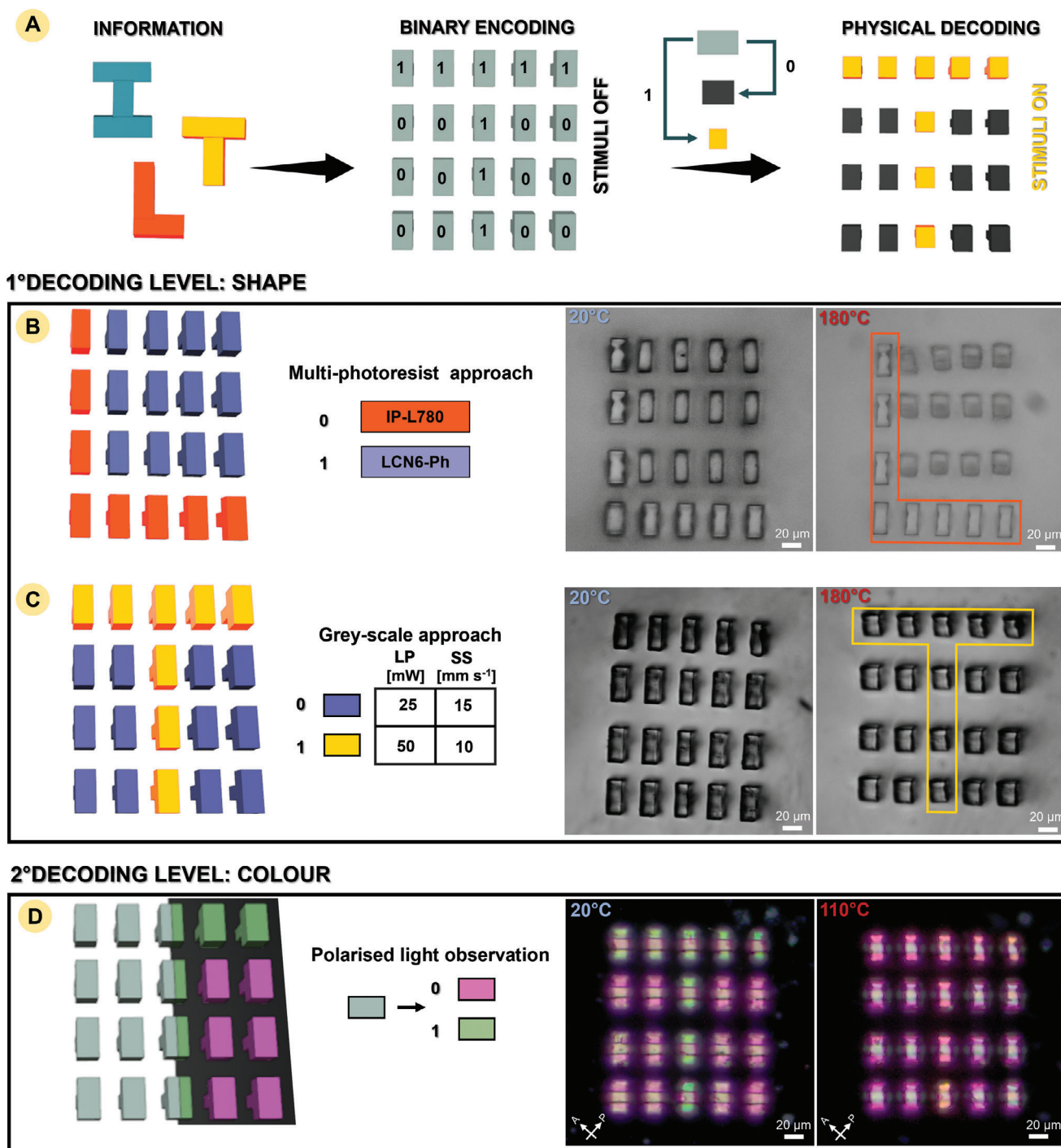
Figure 5. Physical information encoding into a microstructure pixel array. A) Concept for the realization of encoding information as binary code in a pixelated array. Physical revelation is possible under external stimuli; B) Scheme of fabrication of a pixel array by a multi-resist approach and optical images of its realization. LCN6-Ph and IP-L 780 have been used to prepare the pixels that are printed in the same conditions (50 mW and 10 mm s^{-1}). Under thermal revelation, only the LCN pixels undergo a shape deformation; C) Scheme of fabrication of an LCN pixel array by a gray-scale approach and optical images of its realization. LCN6-Ph mixture was printed with different parameters for different pixels (50 mW and 10 mm s^{-1}; 25 mW and 15 mm s^{-1}). Under thermal revelation, the two pixel types contract in a different way; D) Scheme of physical decoding by observation with polarized light and optical images of its realization.

**ADVANCED
SCIENCE NEWS**

www.advancedsciencenews.com

**NANO · MICRO
small**

www.small-journal.com

between pixels. During the heating stage, the selective shrinking of the LCN components (with the others that do not change shape) allows for the information to be clearly revealed.

A second example of letter encoding was realized with a gray scale approach using LCN6-Ph in a single fabrication step as shown in Figure 5C. The micro tables have been printed using two different parameters to maximize the different length under actuation (pixels "0" were printed with 25 mW LP and 15 mm s^{-1} SS, and pixels "1" with 50 mW LP and 10 mm s^{-1} SS). Also in this case, at room temperature, all the pixels were completely indistinguishable and the letter "T" cannot be recognized. Upon heating, all the pixels contracted but with a different extent (as effect of different light dose applied in the fabrication), and making the letter identifiable. An enlarged image of different pixel response created by the gray scale approach is reported in Figure S9 (Supporting Information). For both approaches, once the temperature was cooled down, the letter was hidden again thanks to the process reversibility, as previously discussed. This represents a first decoding level that is based on the physical shape variation of the responsive pixels.

Additionally, when the arrays are observed by POM, another level of identification can be built thanks to the pixel birefringence opening to a multi-level reading of the responsive tag. Observing the sample at 45° with respect to the analyzer, the two kinds of pixels show different colors based on writing parameters. This is a result of the refractive index and block height variation during the fabrication.[57,58] Here, the letter was completely visible at room temperature, but as the temperature increased, the information was hidden, displaying the opposite behavior than in the prior situation. So, for each kind of pixel, it is possible to associate different colors at different temperatures as an additional level of information or secure identification. For the array prepared by the multi-photoresist approach, only the LCN pixels present birefringence (and so the possibility to show different colors) and the letter can be recognized both at room temperatures and higher one.

An overall observation is that the pixelated array can have two different levels of encoding, that are based on two physical mechanisms, one optical (using no polarised or polarized light) and the other due to shape adaptation in response to environmental stimuli such as heating.

Finally, decoding based on physical deformation has also been tested using light. The azo-dye showed a maximum of absorption ≈535 nm, thereby enabling deformation by green light irradiation. Using this stimulus, it was possible to obtain an average of contraction of 33% ± 1% and 22% ± 1%, respectively for the pixels "1" and "0" (Figure S10 and Movie S1, Supporting Information). After switching off the light, the pixels recovered the original shape. The use of light allows to improve the response time of the system from seconds or minutes (such as in the case of temperature, depending on the heating system used) to milliseconds. In our case, the light actuation rate has been estimated as 0.25 ± 0.03 μm ms^{-1} and 0.23 ± 0.02 μm ms^{-1} respectively for the pixels "1" and "0" during the contraction stage and 0.19 ± 0.03 μm ms^{-1} and 0.17 ± 0.03 μm ms^{-1} during the recovery stage. Comparing these labels with other examples of information storage devices, the use of LCN presents some innovative features. In addition to the aforementioned reversibility of the micro-pixel contraction (to enable multiple reading and hiding cycles), we

demonstrated how the double encryption mechanism allow to store a more rich information in the same label. We can encrypt both a letter and a color, not being limited to only one of the two as reported for responsive labels based on emission phenomena or structural color.[59] The dual encryption mechanism can also improve the trustworthiness of labels for multi-level identification. The system speed is in the millisecond scale (using light). Moreover, the few known examples of information encryption based on material shape-change are based on solvent swelling or vapor absorption[60,61] therefore needing a specific environment. In our case, the decoding could be triggered both in air or liquid since it depends only on the material properties and on the external stimulus.

3. Conclusion

We report on the realization of materials with micrometric resolution and programmable actuation that can be controlled by varying fabrication parameters, such as the laser power and the scan speed. We demonstrated the possibility to obtain 3D and suspended micro-objects with increasing degree of complexity and reversible contraction under temperature variation or irradiation with light. First, different reactive LC cross-linkers have been used in the photoresist to determine their impact on the final material properties. During heating, materials containing CL6-Ph presented the best shape-changing properties (with an average maximum contraction of 33%). Moreover, modulating the writing parameters, the maximum deformation can be tuned. This opens the way to one-step fabrication of composite devices having parts that respond in a different way to the same stimulus.

This concept has been applied for a simple system of physical information encryption based on the different shape-change of two kinds of pixels, so the letter is hidden at room temperature and shown under a proper external stimulus. Moreover, the colors that arise from the different pixels by illumination with polarized light can be exploited as a second level of information encoding. In this case, the letter is visible at room temperature and a color difference is decreased by heating. All these effects can be combined together to realize multi-level reading of a responsive tag. Even if this encoding strategy needs further development (e.g., by improving the differences in contraction or by decreasing the actuation temperature), our first demonstration enlarges the range of possible applications of LCN microstructures towards more sophisticated physical information storage devices and opto-mechanical structures with improved functionalities.

4. Experimental Section

Materials: Monomer mixtures contained mesogen C6BP (78% mol/mol), one of the cross-linker CLX-Y (20% mol/mol), Phenylbis(2,4,6-trimethylbenzoyl) phosphine oxide (PBPO, 1% mol/mol) and the acrylate dye (E)−6-((4-((2-Cyano-4-nitrophenyl) diazenyl) phenyl) (ethyl)amino)hexyl acrylate (1% mol/mol). C6BP (4-Methoxybenzoic acid 4-(6-acryloyloxyhexyloxy)phenylester), CL3-Me (1,4-Bis-[4-(3-acryloyloxypropyloxy)benzoyloxy]−2-methylbenzene, also known as RM257) and CL6-Me (1,4-Bis-[4-(6-acryloyloxyhexyloxy)benzoyloxy]−2-methylbenzene also known as RM82) were purchased from Synthon

**ADVANCED
SCIENCE NEWS**

www.advancedsciencenews.com

**NANO · MICRO
small**

www.small-journal.com

Chemicals; and all the other reagents were purchased from Merck. CL6-Ph was synthesized as previously described.[38]

LC Cell Preparation: Microscope cover slips (170 µm thick) were spin coated with a polyimide (grade 5291, type 062B Nissan polyimide Varnish, Nissan Chemical Industries), heated at 90 °C for 1 min and subsequently at 180 °C for 30 min. Then, the coverslips were rubbed unidirectionally with a velvet cloth. Two slides (one circular with a diameter of 24 mm and one square with a width of 16 mm) separated by 50 µm microspheres as spacers were used to build the LC cell. The mixture was heated to the isotropic phase, infiltrated by capillarity in the LC cell, and then cooled to room temperature to achieve a monodomain homogeneous planar alignment.

Direct Laser Writing Fabrication: The 3D structures were created using a commercial DLW workstation, Photonic Professional Nanoscribe GmbH. The system employed a 780 nm, 170 mW femtosecond solid-state laser that generated 120 fs pulses with an 80 ± 1 MHz repetition rate. A 63× objective (NA = 1.4, WD = 190 µm, Zeiss, Plan Apochromat) was used in oil-immersion configuration. A 3D galvo translation stage was used to manage sample location. The LC cell filled with the aligned monomer mixture was placed on the sample holder and a drop of oil (Zeiss Immersol 518F) was applied in the center of the round glass. For all structures, the scan speed (SS) was varied between 10 and 20 mm s^{-1}, the laser power (LP) was modulated between 20 and 50 mW. Slicing distances ranging from 0.1 to 0.5 µm and hatching distances ranging from 0.1 to 0.4 µm were explored. After fabrication, structures were developed in isopropanol (70 °C) to remove remaining unpolymerized photoresist. The 3D structures were designed in Blender and then imported into DeScribe software.

Material Characterization: A thin film for each photoresist was produced by infiltrating LC cells with the mixture followed by polymerization by UV irradiation (385 nm) of the whole cells for 10 min at 25 °C, and 10 min at 45 °C. Phase transition temperatures of mixtures were measured by DSC TA Instruments Calorimeter Q-2000 (TA-Instruments, Milan, Italy) in a nitrogen atmosphere (heating and cooling rate: 20 °C min^{-1}). Polarized Optical Microscopy was performed with a Zeiss Axio Observer A1 microscope in cross-polarized mode equipped with a Linkam PE120 hot stage and an Axio camera. Dynamic Mechanical Analysis was carried out using a Perkin Elmer DMA 8000 in tensile mode.

Microstructures Characterization: SEM was performed using Zeiss Ultra scanning electron microscope, operating at 5 kV under SE2 mode. Prior to imaging, a Au-Pd nano-scale thin layer (≈20 nm) was coated on the polymer structure as a conductive layer under argon atmosphere by sputter coating (Cressington sputter coater 208HR). The Ag-Pd target was purchased from TED PELLA INC. AFM was performed on a commercial SPM system (MFP-3D, Asylum Research, USA) on the micro-fabricated 3D structures. Imaging in air was performed in contact mode at 25 °C.

Supporting Information

Supporting Information is available from the Wiley Online Library or from the author.

Acknowledgements

Conflict of Interest

The authors declare no conflict of interest

Data Availability Statement

The data that support the findings of this study are available from the corresponding author upon reasonable request.

Keywords

[1] C. Ohm, E.-K. Fleischmann, I. Kraus, C. Serra, R. Zentel, *Adv. Funct. Mater.* **2010**, *20*, 4314.
[2] C. M. B. Ho, S. H. Ng, K. H. H. Li, Y.-J. Yoon, *Lab Chip* **2015**, *15*, 3627.
[3] B. Zhou, W. Xu, A. A. Syed, Y. Chau, L. Chen, B. Chew, O. Yassine, X. Wu, Y. Gao, J. Zhang, X. Xiao, J. Kosel, X.-X. Zhang, Z. Yao, W. Wen, *Lab Chip* **2015**, *15*, 2125.
[4] S. Nocentini, D. Martella, C. Parmeggiani, D. S. Wiersma, *Adv. Opt. Mater.* **2019**, *7*, 1900156.
[5] Z. Liu, M. Li, X. Dong, Z. Ren, W. Hu, M. Sitti, *Nat. Commun.* **2022**, *13*, 2016.
[6] M. J. Villangca, D. Palima, A. R. Bañas, J. Glückstad, *Light Sci. Appl.* **2016**, *5*, e16148.
[7] C. Maggi, F. Saglimbeni, M. Dipalo, F. De Angelis, R. Di Leonardo, *Nat. Commun.* **2015**, *6*, 7855.
[8] M. López-Valdeolivas, D. Liu, D. J. Broer, C. Sánchez-Somolinos, *Macromol. Rapid Commun.* **2018**, *39*, 1700710.
[9] A. Sydney Gladman, E. A. Matsumoto, R. G. Nuzzo, L. Mahadevan, J. A. Lewis, *Nat. Mater.* **2016**, *15*, 413.
[10] C. A. Spiegel, M. Hippler, A. Münchinger, M. Bastmeyer, C. Barner-Kowollik, M. Wegener, E. Blasco, *Adv. Funct. Mater.* **2020**, *30*, 1907615.
[11] N. Anscombe, *Nat. Photonics* **2010**, *4*, 22.
[12] A. Selimis, V. Mironov, M. Farsari, *Microelectron. Eng.* **2015**, *132*, 83.
[13] J. Song, C. Michas, C. S. Chen, A. E. White, M. W. Grinstaff, *Macromol. Biosci.* **2021**, *21*, 2100051.
[14] J. Song, C. Michas, C. S. Chen, A. E. White, M. W. Grinstaff, *Adv. Healthcare Mater.* **2020**, *9*, 1901217.
[15] T. Spratte, S. Geiger, F. Colombo, A. Mishra, M. Taale, L.-Y. Hsu, E. Blasco, C. Selhuber-Unkel, *Adv. Mater. Technol.* **2023**, *8*, 2200714.
[16] M. Hippler, E. Blasco, J. Qu, M. Tanaka, C. Barner-Kowollik, M. Wegener, M. Bastmeyer, *Nat. Commun.* **2019**, *10*, 232.
[17] A. Ennis, D. Nicdao, S. Kolagatla, L. Dowling, Y. Tskhe, A. J. Thompson, D. Trimble, C. Delaney, L. Florea, *Adv. Funct. Mater.* **2023**, *33*, 2213947.
[18] J. Qian, S. Kolagatla, A. Pacalovas, X. Zhang, L. Florea, A. L. Bradley, C. Delaney, *Adv. Funct. Mater.* **2023**, *33*, 2211735.
[19] K. M. Herbert, H. E. Fowler, J. M. Mccracken, K. R. Schlafmann, J. A. Koch, T. J. White, *Nat. Rev. Mater.* **2021**, *7*, 23.
[20] C. Ohm, M. Brehmer, R. Zentel, *Adv. Mater.* **2010**, *22*, 3366.
[21] T. Ikeda, J.-I. Mamiya, Y. Yu, *Angew. Chem., Int. Ed.* **2007**, *46*, 506.
[22] M. Del Pozo, L. Liu, M. Pilz Da Cunha, D. J. Broer, A. P. H. J. Schenning, *Adv. Funct. Mater.* **2020**, *30*, 2005560.
[23] M. Winkler, A. Kaiser, S. Krause, H. Finkelmann, A. M. Schmidt, *Macromol. Symp.* **2010**, *291–292*, 186.

[24] H. E. Fowler, P. Rothemund, C. Keplinger, T. J. White, *Adv. Mater.* **2021**, *33*, 2103806.

[25] P.-G. De Gennes, M. Hébert, R. Kant, *Macromol. Symp.* **1997**, *113*, 39.

[26] T. J. White, D. J. Broer, *Nat. Mater.* **2015**, *14*, 1087.

[27] H. Zeng, D. Martella, P. Wasylczyk, G. Cerretti, J.-C. G. Lavocat, C.-H. Ho, C. Parmeggiani, D. S. Wiersma, *Adv. Mater.* **2014**, *26*, 2319.

[28] L. T. De Haan, A. P. H. J. Schenning, D. J. Broer, *Polymer* **2014**, *55*, 5885.

[29] D. Martella, S. Nocentini, D. Nuzhdin, C. Parmeggiani, D. S. Wiersma, *Adv. Mater.* **2017**, *29*, 1704047.

[30] H. Zeng, P. Wasylczyk, C. Parmeggiani, D. Martella, M. Burresi, D. S. Wiersma, *Adv. Mater.* **2015**, *27*, 3883.

[31] S. Nocentini, D. Martella, C. Parmeggiani, S. Zanotto, D. S. Wiersma, *Adv. Opt. Mater.* **2018**, *6*, 1800167.

[32] I. De Bellis, D. Martella, C. Parmeggiani, D. S. Wiersma, S. Nocentini, *Adv. Funct. Mater.* **2023**, *33*, 2213162.

[33] A. Münchinger, L.-Y. Hsu, F. Fürniß, E. Blasco, M. Wegener, *Mater. Today* **2022**, *59*, 9.

[34] I. De Bellis, S. Nocentini, M. G. Delli Santi, D. Martella, C. Parmeggiani, S. Zanotto, D. S. Wiersma, *Laser Photonics Rev.* **2021**, *15*, 2100090.

[35] L.-Y. Hsu, P. Mainik, A. Münchinger, S. Lindenthal, T. Spratte, A. Welle, J. Zaumseil, C. Selhuber-Unkel, M. Wegener, E. Blasco, *Adv. Mater. Technol.* **2023**, *8*, 2200801.

[36] M. Del Pozo, C. Delaney, C. W. M. Bastiaansen, D. Diamond, A. P. H. J. Schenning, L. Florea, *ACS Nano* **2020**, *14*, 9832.

[37] T. Ritacco, D. M. Aceti, G. De Domenico, M. Giocondo, A. Mazzulla, G. Cipparrone, P. Pagliusi, *Adv. Opt. Mater.* **2022**, *10*, 2101526.

[38] S. Donato, D. Martella, M. Salzano De Luna, G. Arecchi, S. Querceto, C. Ferrantini, L. Sacconi, P.-L. Brient, C. Chatard, A. Graillot, D. S. Wiersma, C. Parmeggiani, *Macromol. Rapid Commun.* **2023**, *44*, 2200958.

[39] S. Nocentini, D. Martella, C. Parmeggiani, D. S. Wiersma, *Materials* **2016**, *9*, 525.

[40] A. Grushina, *Adv. Opt. Technol.* **2019**, *8*, 163.

[41] D. Martella, S. Nocentini, C. Parmeggiani, D. S. Wiersma, *Faraday Discuss.* **2020**, *223*, 216.

[42] J.-Y. Wang, F. Jin, X.-Z. Dong, J. Liu, M.-X. Zhou, T. Li, M.-L. Zheng, *Small* **2023**, *19*, 2303166.

[43] G. Decroly, A. Chafaï, G. De Timary, G. Gandolfo, A. Delchambre, P. Lambert, *Adv. Intell. Syst.* **2023**, *5*, 2200394.

[44] Z. Wang, *ACS Nano* **2023**, *17*, 10078.

[45] J. Li, R. Liu, H. Lin, S. Ye, M. Ye, X. Wang, X. Zhu, *X. ACS Appl. Mater. Interfaces* **2021**, *13*, 61536.

[46] Z. Lao, R. Sun, D. Jin, Z. Ren, C. Xin, Y. Zhang, S. Jiang, Y. Zhang, L. Zhang, *Int. J. Extreme Manuf.* **2021**, *3*, 025001.

[47] T. S. Hebner, C. N. Bowman, T. J. White, *Polym. Chem.* **2021**, *12*, 1581.

[48] G. E. Bauman, J. M. Mccracken, T. J. White, *Angew. Chem., Int. Ed.* **2022**, *61*, 1433.

[49] T. Ikeda, J.-I. Mamiya, Y. Yu, *Angew. Chem., Int. Ed.* **2007**, *46*, 506.

[50] M. Yamada, M. Kondo, R. Miyasato, Y. Naka, J.-I. Mamiya, M. Kinoshita, A. Shishido, Y. Yu, C. J. Barrett, T. Ikeda, *J. Mater. Chem.* **2009**, *19*, 60.

[51] L. Dong, Y. Zhao, *Mater. Chem. Front.* **2018**, *2*, 1932.

[52] D. Martella, S. Nocentini, F. Micheletti, D. S. Wiersma, C. Parmeggiani, *Soft Matter* **2019**, *15*, 1312.

[53] I. Dierking, *Textures of Liquid Crystals*, Wiley-VCH, Weinheim, Germany **2003**.

[54] H. Zeng, D. Martella, P. Wasylczyk, G. Cerretti, J.-C. G. Lavocat, C.-H. Ho, C. Parmeggiani, D. S. Wiersma, *Adv. Mater.* **2014**, *26*, 2319.

[55] D. Martella, D. Antonioli, S. Nocentini, D. S. Wiersma, G. Galli, M. Laus, C. Parmeggiani, *RSC Adv.* **2017**, *7*, 19940.

[56] I. Bernardeschi, M. Ilyas, L. Beccai, *Adv. Intell. Syst.* **2021**, *3*, 2100051.

[57] I. De Bellis, D. Martella, C. Parmeggiani, E. Pugliese, M. Locatelli, R. Meucci, D. S. Wiersma, S. Nocentini, *J. Phys. Chem. C* **2019**, *123*, 26522.

[58] Y. Guo, H. Shahsavan, M. Sitti, *Adv. Opt. Mater.* **2020**, *8*, 1902098.

[59] W. Hong, Z. Yuan, X. Chen, *Small* **2020**, *16*, 1907626.

[60] L. Bai, Z. Xie, W. Wang, C. Yuan, Y. Zhao, Z. Mu, Q. Zhong, Z. Gu, *ACS Nano* **2014**, *8*, 11094.

[61] H. Zhang, Q. Li, Y. Yang, X. Ji, J. L. Sessler, *J. Am. Chem. Soc.* **2021**, *143*, 18635.